STAG: Smart Tools and Applications in Graphics (2018)
M. Livesu, G. Pintore and A. Signoroni (Editors)

Indicators Basis for Functional Shape Analysis

S. Melzi[1]

[1]University of Verona, Italy

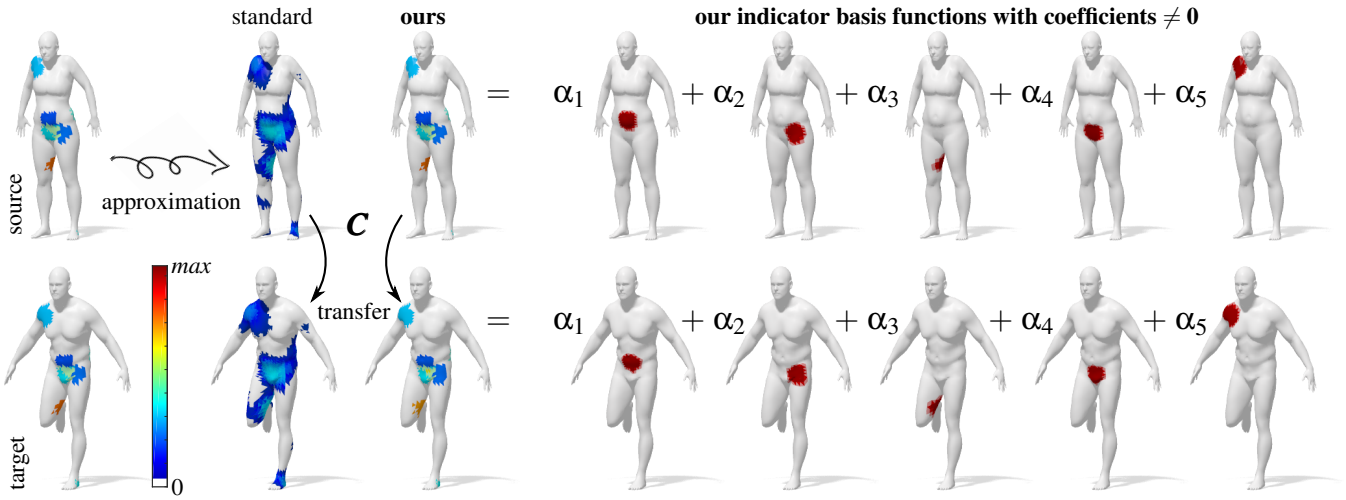

Figure 1: *An example of the proposed indicator basis (IB) and its main applications: the approximation and transfer of a step function. A comparison between standard basis and our IB is proposed on a given function depicted on the left of the Figure (top). From left to right: the original function on the source shape (top) and its ground truth transfer on the target shape (bottom). Approximation (top) and Transfer (bottom) using the standard basis, and using the proposed IB. On the right the linear combination in the proposed basis on the source (top) and on the target shape (bottom). The colormap represents the values of the step function from* 0 *to max. The value* 0 *is represented in white in order to highlight the errors.*

Abstract

Step functions are widely used in several applications from geometry processing and shape analysis. Shape segmentation, partial matching and self similarity detection just to name a few. The standard signal processing tools do not allow us to fully handle this class of functions. The classical Fourier series, for instance, does not give a good representation for these non smooth functions. In this paper we define a new basis for the approximation and transfer of the step functions between shapes. Our definition is fully spectral, allowing for a concise representation and an efficient computation. Furthermore our basis is specifically built in order to enhance its use in combination with the functional maps framework. The functional approach also enable us to handle shape deformations. Thanks to that our basis achieves a large improvement not only in the approximation of step functions but also in the transfer, exploiting the functional maps framework. We perform a large set of experiments showing the improvement achieved by the proposed basis in the approximation and transfer of step functions and its stability with respect to non isometric deformations.

CCS Concepts

•***Computing methodologies*** → ***Shape analysis;*** *Shape modeling;* •***Mathematics of computing*** → *Functional analysis;*

1. Introduction

In the era of automation, the need of ability for the computers to explore the real world has been growing exponentially. This is mainly due to the wide availability of algorithms and devices for the acquisition and generation of geometric data from the real word. These geometric data are digital representation of the surfaces of objects,

DOI: 10.2312/stag.20181300

animals and people from reality. In the last decades the interest in these geometric data has greatly grown thanks to the several applications in which they are involved. Some of these applications are acquisition, reconstruction, analysis, manipulation, simulation and transmission of complex 3D models. Working with digital representations of real objects, we still have to face many issues related to their deformations. The real world is indeed not rigid and most of the shapes can be found under different *non rigid deformations*. One of the possible approaches to deal with these non rigid deformations is the *functional maps framework* proposed by Ovsjanikov et al. in [OBCS*12a]. The main idea of functional maps is to connect two surfaces representing correspondences between functions defined on them instead of correspondences between their points. Moving in the functional spaces the problems related to the non-rigid deformations of the surfaces are solved or at least simplified. The functional space defined on surfaces is usually represented as the space spanned by a fixed finite set of basis functions. In this context the widely adopted basis is the *Fourier basis*, that has been shown to be optimal for the representation of continuous functions. Recently many researches have been dedicated to the definition of a new basis or a new representation for the functional space. In this paper we propose the *Indicator basis* (IB), a new basis for the approximation and the transfer of a specific set of functions defined on manifolds: the *step functions*. Given a manifold $\mathcal{M}$ a *step function* on $\mathcal{M}$ is defined as every finite linear combination of region indicator functions. Where a region indicator function of a given region $R \subset \mathcal{M}$ is a function f such that:

$$f : \mathcal{M} \longrightarrow \{0,1\}, \tag{1}$$

and $f(x) = 1$ if $x \in R$ while $f(x) = 0$ otherwise. These functions are very simple and they can be found in several applications in geometry processing. An example is shape segmentation, in which the shape is subdivided in regions each of which generates a step in a step function. Another example in which step functions could be useful is partial matching, where only a region of one shape could be correctly matched with another shape.

These step functions are not continuous, therefore the Fourier basis does not appear to be appropriate in this case. For all these reasons it is necessary to provide a good representation for step functions. In this paper we propose a new basis for the step functions representation. The proposed basis is spectrally defined exploiting the strength of the spectral properties of the shapes. In particular the spectral approach allows us to obtain a concise and efficient formulation. This formulation is also suitable for use in conjunction with the functional maps framework obtaining directly the transfer of functions between shapes.

The main contributes of this paper are:

- We analyze the family of functions defined on surfaces that corresponds to standard step functions defined on 1D real interval.
- We define the *Indicator Basis* as a novel alternative for the synthesis and analysis of the step functions on surfaces.
- We propose an efficient algorithm for the construction of the *Indicator Basis*.
- We prove and evaluate how the spectral based definition is well suited for the transfer of step functions between shapes.
- We compare the proposed basis with the state of the art method in functional space representation on manifolds.
- We compare our method with a geodesic and a heat based alternatives, proposed here for the first time, that can naturally be identified as competitors to the proposed approach.

The method proposed in this paper could really contribute to many applications in geometry processing.

The rest of the paper is organized as follows. In Section 2 we are going to introduce the state of art in functional representation and signal processing on manifolds. An overview and motivations for the proposed framework are summarized in Section 3. Section 4 is devoted to the theory and implementation of the *Indicator Basis*. Experiments and evaluation of the method in standard applications are then collected in Section 5. Finally Sections 6 contains the conclusions of the paper.

2. Related work

Signal processing is the collection of all the technologies for representation, manipulation and transformation of signals. A key question in signal processing is how we should represent a signal. The desired representation must be precise, concise and must simplify operations on signals. One of the widely adopted representation is the Fourier Transform. The Fourier transform was proposed by Joseph Fourier [Fou07], in 1807. Namely we refer to this representation as the *Fourier transform* also referred as the frequency representation of the original signal. This frequency representation is obtained thanks to the *Fourier basis*, a set of functions that can be computed as the eigenvectors of a standard operator: the *Laplace operator*. Given a signal defined on a domain, such as time, the Fourier transform represents the signal as the linear combination of the frequencies that generate it.
In Geometry processing we are interested in studying signals defined on non Euclidean domain such as 2-dimensional surfaces of real objects embedded in the 3D space. This kind of domains are approximated and modelled as a smooth compact connected Riemannian surface $\mathcal{M}$ (possibly with a boundary $\partial\mathcal{M}$) embedded into $\mathbb{R}^3$. We refer the reader to [dC92] for a deeper introduction to Riemannian manifolds.
In order to extend signal processing to the non Euclidean domains we need to define several tools for the analysis of signals defined on surfaces. All the theory involved in these definitions are out of the scope of this paper. The *Laplace-Beltrami operator* (LBO) is a positive semi-definite operator that generalizes the corresponding notion of Laplace operator from Euclidean spaces to manifolds. By analogy with the Euclidean Fourier transform the eigenfunctions of LBO form an orthonormal basis for signals defined on surfaces [Tau95], [VL08]. The LBO has been involved in several applications as shown in [Lév06] giving rise to the spectral approaches in the computer graphic. Some of the contributes arise directly from the LBO are the global point signatures [Rus07], and shape DNAs [RWP06]. Diffusion process defined on manifolds and all its derivations are strictly related to LBO and spectral geometry processing: the diffusion distances [CL06], the heat kernel signature [SOG09, GBAL09] and the wave kernel signatures [ASC11]. In 2012 Ovsjanikov et al. [OBCS*12a] introduced the functional maps paradigm to represent correspondences between functional spaces instead of correspondences between points on the surfaces. During last years many improvements to the functional

maps framework have been proposed in particular in [NO17] the authors showed how it is possible to obtain a huge improvement in the functional maps estimation representing descriptors as linear operators acting on functions through pointwise multiplication. Similarly to theirs, Nogneng et al. [NMR*18] shown how a given functional map can be exploited representing the functional spaces not only as linear combinations of the LBO eigenfunctions but also involving their (possibly high-order) point-wise products. The functional maps framework is as well strictly related with the LBO, the LBO eigenfunctions are indeed adopted as basis for the functional spaces. In [ABK15] Aflalo et al. show how the choice of the LBO eigenfunctions are optimal for the representation of continuous functions with bounded variation. Usually only a few subset of the LBO eigenfunctions (the ones with smaller eigenvalues) are used as truncated basis for the functional space. This choice constitutes the main limitation of the LBO eigenfunctions, in fact the set of the eigenfunctions used represents only the low-frequencies and it is not able to represent functions with fast variations. Furthermore the LBO eigenfunctions from two different shapes suffer of switches in the signs and in the order that they take from the corresponding eigenvalues, also in the case of near-isometric shapes, as deeply investigated in [SK14]. To solve these issues Kovnatsky et al. proposed the construction of compatible basis on collections of shapes using simultaneous diagonalization of Laplacians [KBB*13]. Another drawback of LBO eigenfunction is that they are globally defined. Using the LBO eigenfunctions it is not possible to localize the analysis on small regions on the shape. Tools for the spectral local analysis on non-Euclidean manifolds, have recently been proposed: the Windowed Fourier Transform (WFT) for graphs [SRV12] and shapes [BMM*15] together with an anisotropic version [MRCB16] defined on the eigenfunctions of the Anisotropic LBO [ARAC14]. These methods try to localize the analysis of signals, but LBO eigenfunctions are still adopted as a basis for the spectral representation. Neumann et al. [NVT*14] applied the approach of [OLCO13] to problems in computer graphics. In [NVT*14] authors proposed the compressed manifold modes which provides a new basis locally supported. As suggested in [OLCO13], the compressed modes are the solutions of an optimization problem that combines the Dirichlet energy with a sparsity-inducing regularization based on L_1-norm. An alternative and more efficient computation of the compressed modes is provided by Kovnatsky et al. [KGB16]. The main limitation of this approach is that it does not provide the ability to select the region in which the modes are localized. A recent approach proposed by Choukroun et al. [CSBK17] considers the spectral decomposition of an hamiltonian operator realized as a small modification to the classic LBO. In [MRCB18] Melzi is proposed a similar solution that provides a basis simultaneously localized and orthogonal to the global LBO eigenbasis. As in the classical signal processing, different basis can be exploited in order to face different issues or depending on the final application. Basis and frames proposed in [OLCO13] , [KBB*13], [NMR*18], [CSBK17], [MRCB18] are all alternatives to the standard Fourier basis [VL08]. The key idea of this paper is to propose the *Indicator Basis* (IB), a new alternative for signal processing on manifold. The novelty of this basis is that it is specifically defined for *step functions*. These functions are not continuous and our definition is likewise not continuous. The IB improves the approximation the transfer of step functions between different shapes exploiting the functional maps framework. Our experiments highlight that the proposed basis is able to handle shape deformations and bring several advantages in various applications.

3. Overview

1D Euclidean Domain. Here we provide a general idea of the contents of this paper, showing the motivations in the case of 1D Euclidean domain. In this domain the Fourier basis is composed by the harmonic functions corresponding to the eigenfunctions of the Laplace operator. The Laplace operator can then be seen as the sum of second partial derivatives of the function. This basis is optimal for the analysis and the synthesis of smooth functions with limited variations.

In this paper we would like to improve the approximation and transfer of a specific class of functions: the *step functions*. More formally the step functions can be defined as the set of all possible finite linear combination of indicator functions. An example of an indicator function f_R is the following:

$$f_R : \mathcal{D} \longrightarrow \mathbb{R} \quad | \quad f_R(x) = \begin{cases} 1, & \text{if } x \in R \\ 0, & \text{otherwise} \end{cases} \tag{2}$$

where $R \subseteq \mathcal{D}$ is an interval in the domain. Given a set of interval $\{R_1, \ldots, R_q\}$ and the corresponding indicator functions $\{f_{R_1}, \ldots, f_{R_q}\}$ a *step function* s is any linear combination of them:

$$s : \mathcal{D} \longrightarrow \mathbb{R} \quad | \quad s = \alpha_1 f_{R_1} + \ldots + \alpha_q f_{R_q}, \tag{3}$$

where $\alpha_1, \ldots, \alpha q \in \mathbb{R}$. For simplicity here we consider only connected interval on the real line, if one of the interval is composed by more than one connected component we can easily divide this interval in all its connected components and consider one indicator function for each of them. A step function is clearly a not smooth function and therefore the Fourier basis is not an optimal choice for represent this functions.

For this reason we propose the *Indicator Basis* (IB) a new basis, specifically defined to approximate and transfer indicator functions. The main contribute of this paper is to define a set of indicator functions satisfying the following properties:

1. All the step functions can be well approximated as a linear combination of these functions.
2. The set is finite, providing a concise and efficient representation.
3. The definition and computation of these functions should be efficient.
4. The obtained representation of step functions must be easily transferred between different domains.

Some examples of Fourier basis functions and some of Indicator basis functions are shown in Figure 2.

2-dimensional surfaces. Once we get the general idea in the 1D Euclidean domain, we focus on the case of 2-dimensional surfaces embedded in $\mathbb{R}^3$. A surface of this kind is modelled as a connected compact smooth 2-dimensional Riemannian manifold $\mathcal{M} \subset \mathbb{R}^3$, eventually with a boundary $\partial\mathcal{M}$. In the discrete setting we represent $\mathcal{M}$ as a triangular mesh with a set of $n_{\mathcal{M}}$ vertices $\mathcal{V}$ and vertices $\mathcal{E}$.

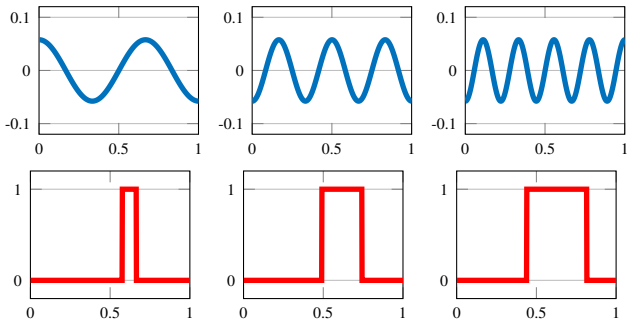

Figure 2: *Three Fourier basis functions (top row) and three Indicator basis functions (bottom row) in 1D under Neumann boundary conditions.*

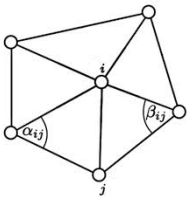

Thanks to the differential geometry definitions we are able to equip the surface $\mathcal{M}$ with the *Laplace Beltrami Operator* (LBO), the second order differential operator that can be seen as the counterpart of the Laplace operator on manifolds. Due to lack of space we refer to [dC92] for more details on the differential geometry theory involved in the definition of the LBO.

In the discrete setting the LBO is represented as a matrix of dimension $n_{\mathcal{M}} \times n_{\mathcal{M}}$. This matrix is obtained as the product $\mathbf{\Delta}_{\mathcal{M}} = (\boldsymbol{A}^{\mathcal{M}})^{-1}\boldsymbol{W}^{\mathcal{M}}$. $\boldsymbol{A}^{\mathcal{M}}$ is the *mass matrix* a diagonal matrix which entries are equal to the area element associated to each vertex. $\boldsymbol{W}^{\mathcal{M}}$ is the *stiffness matrix* defined accordingly to the local geometry of the surface. More explicitly the *stiffness matrix* $\mathbf{W}_{\mathcal{M}}$ contains the *cotangent weights* w_{ij} defined as follows:

$$w_{ij} = \begin{cases} (\cot\alpha_{ij} + \cot\beta_{ij})/2 & ij \in \mathcal{E}_i \subset \mathcal{E}; \\ (\cot\alpha_{ij})/2 & ij \in \mathcal{E}_{\partial\mathcal{M}} \subset \mathcal{E}; \\ -\sum_{k\neq i} w_{ik} & i = j; \\ 0 & \text{else}; \end{cases} \tag{4}$$

where α_{ij}, β_{ij} denote the angles $\widehat{ikj}, \widehat{jhi}$ of the triangles sharing the edge ij, $\mathcal{E}_i$ are the edges connected to the vertex i and $\mathcal{E}_{\partial\mathcal{M}}$ are the edges on the boundary (see inset Figure where the adopted notation is clarified). To better understand the previous construction and to see details in these choices we refer to [PP93].

Since the LBO is a positive semidefinite operator $\mathbf{\Delta}_{\mathcal{M}}\colon \mathcal{F}(\mathcal{M},\mathbb{R}) \to \mathcal{F}(\mathcal{M},\mathbb{R})$, it admits an eigendecomposition $\mathbf{\Delta}_{\mathcal{M}}\boldsymbol{\phi}_l = \lambda_l\boldsymbol{\phi}_l$, where $\lambda_1 \leq \lambda_2 \leq \ldots$ are real eigenvalues, and $\boldsymbol{\phi}_1, \boldsymbol{\phi}_2, \ldots$ are the corresponding eigenfunctions. These eigenfunctions can be seen again as the counterpart of the Fourier basis on manifolds. Even in this case the Fourier basis is composed by smooth functions and as shown in [ABK15] it is optimal for the representation of smooth functions defined on surfaces.

A step function on $\mathcal{M}$, the main character of this paper, can be defined as a finite linear combination of indicator functions. An indicator function on $\mathcal{M}$ is a function f_R such that:

$$f_R : \mathcal{M} \longrightarrow \mathbb{R} \quad | \quad f(x) = \begin{cases} 1, & \text{if } x \in R \\ 0, & \text{otherwise} \end{cases} \tag{5}$$

where $R \subseteq \mathcal{M}$ is a given region inside $\mathcal{M}$. Given a set of regions in $\mathcal{M}$ $\{R_1, \ldots, R_q\}$ and the corresponding indicator functions $\{f_{R_1}, \ldots, f_{R_q}\}$, $s = \alpha_1 f_{R_1} + \ldots + \alpha_q f_{R_q}$ $(\alpha_1, \ldots, \alpha q \in \mathbb{R})$ is a *step function* on $\mathcal{M}$. As in the 1D case, we consider for simplicity connected regions on the surfaces only. Fourier basis and indicator basis examples on a 2-dimensional surface is depicted in Figure 3.

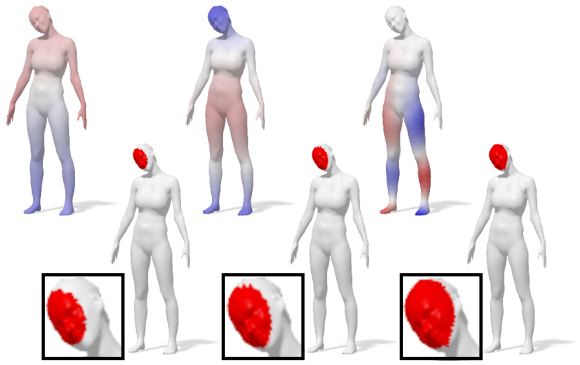

Figure 3: *Three Fourier basis functions (top row) on a 2-dimensional surface of a human body and three Indicator basis functions (bottom row) on the same human shape. The differences between the three selected τ are highlighted in the black box on the bottom of the Figure.*

Once again the Fourier basis is not well defined for the representation of the step functions. In this paper we propose the *Indicator basis* for the approximation and the transfer of step functions between surfaces. The properties that we list for the 1D case can be summarized saying that with the Indicator basis we obtain an efficient and concise representation of step functions that can be naturally involved in the functional maps framework [OBCS*12b], improving our ability to transfer step functions between shapes.

4. Method

In this Section we introduce the implementation of the IB on shapes. The Section is divided in two parts. The first is devoted to the definition of the IB on a single shape. In the second part we focus on the transfer of the IB between two given shapes.

4.1. Computation of the Indicator basis on a single shape

Let $\mathcal{M}$ be a shape with its mass matrix $\boldsymbol{A}^{\mathcal{M}}$ and its LBO eigendecomposition:

$$\Lambda^{\mathcal{M}} = \left\{\lambda_1^{\mathcal{M}}, \ldots, \lambda_{k_{\mathcal{M}}}^{\mathcal{M}}\right\} \text{ the set of eigenvalues and}$$
$$\mathbf{\Phi}^{\mathcal{M}} = \left\{\boldsymbol{\phi}_1^{\mathcal{M}}, \ldots, \boldsymbol{\phi}_{k_{\mathcal{M}}}^{\mathcal{M}}\right\} \text{ the corresponding eigenfunctions,}$$

both truncated to dimension $k_{\mathcal{M}}$.

The IB on $\mathcal{M}$ is obtained accordingly to the following pipeline.

Compute the Subset of Vertices. Given the mesh associated to $\mathcal{M}$ and its set of vertices $\mathcal{V}$ we want to select a subset $\mathcal{V}_{IB}$ of $\mathcal{V}$. The only property we need to take care of is to select vertices uniformly distributed on the surface guaranteeing to cover the entire shape. To do that we adopt the *fast marching farthest point sampling* algorithm [MD03, ELPZ97], based on the geodesic distances. In all

the experiments, where it is not specified, we select the 5% of the vertices. We denote the number of selected vertices as $n_{IB} < n_{\mathcal{M}}$. An example of the obtained set of vertices on a human shape is depicted on the left of Figure 5.

Spectral Gaussian. In order to build our IB we need to define indicator functions on $\mathcal{M}$. This definition should be general and specifically designed for approximation and transfer of step functions. For both this goals we focus on the spectral representation of functional space defined on surfaces. The idea is to define a Gaussian in the spectral domain. In other words we define a Gaussian function as its coefficient in the Fourier representation. To define the spectral Gaussian two parameters should be selected: the center and the spread of the spectral Gaussian. We fix $\lambda_1 = 0$ as the spectral center of the Gaussian and $\tau \in \mathbb{R}^+$ for the spread. Then for each frequency

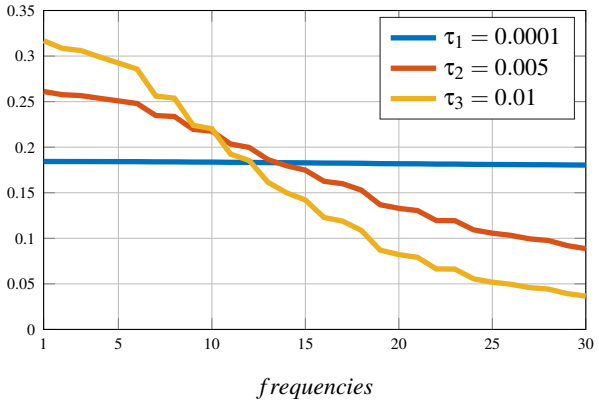

Figure 4: *The spectral Gaussian* $\widehat{\boldsymbol{g}}^{\tau_1}, \widehat{\boldsymbol{g}}^{\tau_2}, \widehat{\boldsymbol{g}}^{\tau_3}$ *computed for* $\tau_1 = 0.0001, \tau_2 = 0.005$ *and* $\tau_3 = 0.01$.

the coefficient of the spectral Gaussian is defined as:

$$\widehat{\boldsymbol{g}}_l = e^{-\tau(\lambda_l - \lambda_1)}, \tag{6}$$

varying l in the set of adopted frequencies: $l \in \{1, \dots, k_{\mathcal{M}}\}$. The function defined in this way associates a values on each frequency from 1 to $k_{\mathcal{M}}$. Three examples corresponding to three different choices of τ are depicted in Figure 4, where the x-axis represents the frequencies, and the values of the Gaussians are represented on the y-axis. The spatial image of this spectral Gaussian is a Gaussian again which depends on the choice of a point $x \in \mathcal{M}$ that is the center of the Gaussian $\boldsymbol{g}_x$ computed as follows:

$$\boldsymbol{g}_x = \sum_{l=1}^{k_{\mathcal{M}}} (\widehat{\boldsymbol{g}}_l \odot \boldsymbol{\phi}_l(x)) \boldsymbol{\phi}_l, \tag{7}$$

where $\odot$ is the element-wise products. The values $(\widehat{\boldsymbol{g}}_l \odot \boldsymbol{\phi}_l(x)), \forall l \in \{1, \dots k_{\mathcal{M}}\}$ can be seen as the spectral coefficients in the basis $\boldsymbol{\Phi}^{\mathcal{M}}$ of $\boldsymbol{g}_x$. We compute the spatial Gaussian on each of the points in the set $\mathcal{V}_{IB} = \{p_1, \dots, p_{n_{IB}}\}$. The width of the the spectral Gaussian depends on the parameter τ. Larger is the value of τ tighter is the spectral Gaussian. We select a set T of 3 different τ, $T = \{\tau_1 = 0.001, \tau_2 = 0.005, \tau_3 = 0.01]\}$. With these parameters we obtain $q = 3 \times n_{IB}$ spatial Gaussian that are collected side by side in a matrix $\boldsymbol{G} = [\boldsymbol{g}_{p_1}^{\tau_1}, \dots, \boldsymbol{g}_{p_1}^{\tau_3}, \dots, \boldsymbol{g}_{p_{n_{IB}}}^{\tau_1}, \dots, \boldsymbol{g}_{p_{n_{IB}}}^{\tau_3}]$

Our definition of the IB functions is completely related with the Fourier Basis obtained from the eigendecomposition of the LBO. This spectral definition is general (it does not depend on specific properties of the mesh). The LBO is completely intrinsic, being fully defined by the metric tensor. The space of functions spanned by the first eigenfunctions of the LBO are stable under near-isometries as shown for example in the work of [Kat95]; therefore the LBO eigenbasis is well designed for the transfer between pairs of shapes as a low-pass representation of signals, as shown in []. The definition of the Gaussian in the spectral domain has been already exploited in many works from graph theory and geometry processing. Shuman et al proposed in [SRV12] the spectral Gaussian definition as a part of the framework that defines the windowed Fourier transform on graphs. Extending the work of Shuman from graphs to manifold in [BMM*15] the spectral Gaussian are used in order to define a window function for the convolution on the manifold. This window is a key component of the convolutional neural network defined on manifold that are proposed in [BMM*15]. The same definition is exploited in [MRCB16] where an anisotropic version of the windowed Fourier transform for manifolds is proposed [ABK15]. Here we report the formula that defines the spectral Gaussian and we refer to previous works for more details.

Some spatial Gaussian obtained from this definition varying the value of τ and with two different center are shown in the middle of Figure 5.

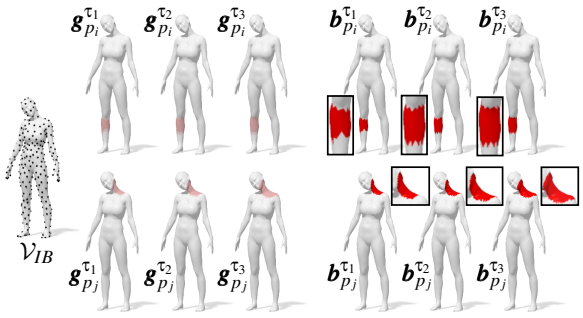

Figure 5: *An overview of the steps in the definition of the Indicator basis. From left to right, the points selected on* $\mathcal{M}$*, spatial Gaussian defined for the 3 different* τ *values around two different points (one on the first row and one on the second row), finally the indicator basis functions obtained from the previous Gaussian functions. Near to each example we add a zoom on then region where the indicator is localized.*

From Gaussian to Indicator function. Finally for each of the Gaussian function $\boldsymbol{g}_x^{\tau}$, in order to obtain the indicator function that compose the proposed basis IB, we perform the following post-processing:

Normalization: $\boldsymbol{g}_x^{\tau} = \frac{|\boldsymbol{g}_x^{\tau}|}{max(|\boldsymbol{g}_x^{\tau}|)}$.
Saturation: $\boldsymbol{b}_x^{\tau}(p) = 1$ if $\boldsymbol{g}_x^{\tau}(p) > \gamma$.
Remove noise: $\boldsymbol{b}_x^{\tau}(p) = 0$ if $\boldsymbol{g}_x^{\tau}(p) < \gamma$.

We refer to the last two steps as binaryzation of the basis functions. In our experiments we fix $\gamma = \frac{3}{4}$. After this post-processing each of the original spatial Gaussian becomes a binary indicator function. We collect all of this indicator functions side by side in the basis

Algorithm 1 Indicator Basis computation on $\mathcal{M}$.

Input: $\mathcal{M}$ the mesh with its Fourier basis $\mathbf{\Phi}^{\mathcal{M}}$,
a set of real values $T = \{\tau_1, \dots \tau_t\}$, and a threshold $\gamma \in (0,1)$.
Output: $\mathcal{I} = \{\boldsymbol{b}_1, \dots, \boldsymbol{b}_q\}$ Indicator basis on $\mathcal{M}$.

```
Select a subset of n_IB vertices V_IB ⊂ V.
for j = 1 : t do
    Compute ĝ^{τ_j} the spectral Gaussian.
    for i = 1 : n_IB do
        Compute g_{p_i}^{τ_j} the spatial Gaussian translated in v_i.
        Normalization step: g_{p_i}^{τ_j} = |g_{p_i}^{τ_j}| / max(|g_{p_i}^{τ_j}|).
        Compute b_{p_i}^{τ_j} as binaryzation of g_{p_i}^{τ_j} w.r.t. the threshold γ.
    end for
end for
return I = {b_1 = b_{p_1}^{τ_1}, ..., b_q = b_{p_{n_IB}}^{τ_t}}
```

matrix $\mathcal{I}$. When it is necessary we will refer to this basis as $\mathcal{I}^{\mathcal{M}}$ making explicit the surface on which it is defined.

The pipeline for the construction of the indicator basis is summarized in Algorithm 1.

4.2. Approximation of a Function with $\mathcal{I}$

Once we have our basis $\mathcal{I}$, given a function f we want to approximate f as $\tilde{f}$ a linear combination of the basis function in $\mathcal{I}$ that means:

$$\tilde{f} = \mathcal{I}\boldsymbol{\alpha}^f,$$

where $\boldsymbol{\alpha}^f$ are the coefficients of f in the basis $\mathcal{I}$. The computation of $\boldsymbol{\alpha}^f$ can be defined in different way, here we propose two alternatives. The first is to compute $\boldsymbol{\alpha}^f$ as the solution of the following linear system:

$$\mathcal{I}\boldsymbol{\alpha}^f = f. \tag{8}$$

Unfortunately the basis in $\mathcal{I}$ are not linear independent and the previous linear system is usually underdetermined. As a valid choice we propose to compute $\boldsymbol{\alpha}^f$ as the solution of the following minimization problem:

$$\boldsymbol{\alpha}^f = \underset{\boldsymbol{\alpha}\in\mathbb{R}^q}{\arg\min} \|\mathcal{I}\boldsymbol{\alpha} - f\| + \rho\|\boldsymbol{\alpha}\|_0. \tag{9}$$

The minimization of the $l0$ pseudo-norm promotes the sparsity of the solution and in particular promotes solutions with a larger number of zeros. This is a good choices for our basis; in fact we have a lot of basis functions and we know that just a few of them are needed to obtain a good approximation of the signal. In our implementation we use the method proposed in [RZE08] for the minimization of the $l0$ pseudo-norm. We fix the parameter $\rho = 0.75$. An approximation example on the 1D Euclidean case is shown in Figure 6. As can be seen the proposed basis (in red) allows to better approximate the original step function (in black) with respect to the results obtained using the standard Fourier basis (in blue). We propose 2 different signals. On the left the approximation of a binary ($\{0,1\}$) step function. On the right results on a similar step function, but with values different from 0 and 1. An example of the approximation of a function between two 2-dimensional surfaces using the proposed basis is depicted in the first row of Figure 1, with a comparison with the standard approach based on the LBO eigenbasis.

4.3. Transfer of a Function with IB

Finally we consider the case in which we have two shapes $\mathcal{M}$ and $\mathcal{N}$ with their LBO eigenbasis $\mathbf{\Phi}^{\mathcal{M}} = \left\{\boldsymbol{\phi}_0^{\mathcal{M}}, \dots, \boldsymbol{\phi}_{k_{\mathcal{M}}-1}^{\mathcal{M}}\right\}$ and $\mathbf{\Phi}^{\mathcal{N}} = \left\{\boldsymbol{\phi}_0^{\mathcal{N}}, \dots, \boldsymbol{\phi}_{k_{\mathcal{N}}-1}^{\mathcal{N}}\right\}$ truncated to dimension $k_{\mathcal{M}}$ and $k_{\mathcal{N}} \in \mathbb{N}$ respectively. One of the main applications in signal representation is functions transfer between two different domains. The transfer of step functions is the main application that we face with our basis $\mathcal{I}$.

Functional Maps. As already said we make use of the Functional maps framework [OBCS*12a] to transfer functions between shapes. Here we just give a short introduction to the original framework, and we refer to [OBCS*12a] for details. Consider $\pi : \mathcal{N} \to \mathcal{M}$ be a pointwise map between $\mathcal{N}$ and $\mathcal{M}$. The functional maps framework [OBCS*12a] proposes to consider a linear operator $T : \mathcal{F}(\mathcal{M},\mathbb{R}) \to \mathcal{F}(\mathcal{N},\mathbb{R})$ that maps functions from $\mathcal{N}$ to $\mathcal{M}$, defined as the composition $T(f) = f \circ \pi$. Adopting to the LBO eigenbasis, the operator T, namely the *functional map*, admits a matrix representation $\mathbf{C} = (c_{ij})$, which coefficients can be obtained as:

$$T(f) = T\sum_i \langle f, \boldsymbol{\phi}_i^{\mathcal{M}}\rangle_{\mathcal{M}} \boldsymbol{\phi}_i^{M} = \sum_{ij} \langle f, \boldsymbol{\phi}_i^{\mathcal{M}}\rangle_{\mathcal{M}} \underbrace{\langle T\boldsymbol{\phi}_i^{\mathcal{M}}, \boldsymbol{\phi}_j^{\mathcal{N}}\rangle_{\mathcal{N}}}_{c_{ji}}, \tag{10}$$

Accordingly to what is suggested in [OBCS*12a] we use only truncated set of eigenbasis, thus we also truncate the series (10). This choice reduces the estimation of the functional map to a smaller matrix $\mathbf{C} \in \mathbb{R}^{k_{\mathcal{N}} \times k_{\mathcal{M}}}$. In this work we consider the map $\boldsymbol{C}$ to be given for all the methods that we compare. We refer for the different possible solutions for the estimation of the map to the literature collected in Section 2.

Mapping of the Gaussian. As we saw previously the Gaussian functions on $\mathcal{M}$ are defined through their spectral coefficients. If we consider a Gaussian function $\boldsymbol{g}_x^{\tau}$ its spectral coefficients are $\{\widehat{\boldsymbol{g}}_l^{\tau} \odot \boldsymbol{\phi}_l(x)\}_{l=1}^{k_{\mathcal{M}}}$ that correspond to their representation in the Fourier basis. Exactly these coefficients are the ones that can be transferred by the functional map $\boldsymbol{C}$. Indeed thanks to $\boldsymbol{C}$ we can compute the spectral coefficients for the Gaussian functions on $\mathcal{N}$:

$$\boldsymbol{C}[\widehat{\boldsymbol{g}}_1^{\tau} \odot \boldsymbol{\phi}_1(x), \dots, \widehat{\boldsymbol{g}}_{k_{\mathcal{M}}}^{\tau} \odot \boldsymbol{\phi}_{k_{\mathcal{M}}}(x)]^{\top}. \tag{11}$$

Thus for every τ and every $x \in \mathcal{M}$ we can compute the image of g_x^{τ} on $\mathcal{N}$ as:

$$\boldsymbol{h}_x^{\tau} = \mathbf{\Phi}^{\mathcal{N}}\boldsymbol{C}[\widehat{\boldsymbol{g}}_1^{\tau} \odot \boldsymbol{\phi}_1(x), \dots, \widehat{\boldsymbol{g}}_{k_{\mathcal{M}}}^{\tau} \odot \boldsymbol{\phi}_{k_{\mathcal{M}}}(x)]^{\top}. \tag{12}$$

The notation $\mathbf{h}_x^{\tau}$ with the point $x \in \mathcal{M}$ as subscript can be misleading. In fact being a function defined on $\mathcal{N}$ the correct center of the Gaussian $\boldsymbol{h}_x^{\tau}$ should be a point $y \in \mathcal{N}$ such that $y = \pi^{-1}(x)$ the correspondent point of $x \in \mathcal{M}$. Varying the value of $\tau \in T$ and varying the point x in the set $\mathcal{V}_{IB}$ we obtain $\boldsymbol{H} = [\boldsymbol{h}_{p_1}^{\tau_1}, \dots, \boldsymbol{h}_{p_1}^{\tau_3}, \dots, \boldsymbol{h}_{p_{n_{IB}}}^{\tau_1}, \dots, \boldsymbol{h}_{p_{n_{IB}}}^{\tau_3}]$ the images of the set of spatial Gaussian $\boldsymbol{G}$. Each of the functions in $\boldsymbol{H}$ is in correspondence with its pre-image in the same position in $\boldsymbol{G}$.

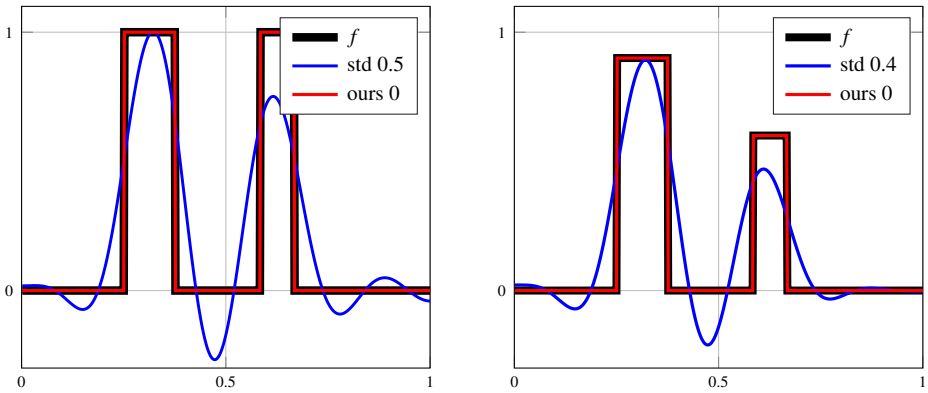

Figure 6: *We compare the approximation of a step function (in black) using the standard harmonics (in blue) and the proposed indicator basis (in red). On the left we compare the approximation of a function with values in $\{0,1\}$. On the right a similar step function with non integer values. In the legend on the right side of the name we report the relative error for each method.*

From $\boldsymbol{H}$, the set of Gaussian on $\mathcal{N}$, following the same binaryzation step performed on $\boldsymbol{G}$, we are able to obtain the indicator basis $\mathcal{I}^{\mathcal{N}}$. Thanks to the ordered correspondence between the columns in $\mathcal{I}^{\mathcal{M}}$ and the ones in $\mathcal{I}^{\mathcal{N}}$ we can transfer the function $f \in \mathcal{F}(\mathcal{M},\mathbb{R})$ on $\mathcal{N}$ easily as:

$$g = \mathcal{I}^{\mathcal{N}} \boldsymbol{\alpha}^{f} \,, \tag{13}$$

where $\boldsymbol{\alpha}^{f}$ are the same coefficients that represent f in the basis $\mathcal{I}^{\mathcal{M}}$, computed as in Equation 9. Thanks to its formulation the computation of the proposed basis is well defined w.r.t. the functional maps, so it is specifically built to exploit the transfer of function with the functional maps $\boldsymbol{C}$. An example of the transfer of a function between two different shapes using the proposed basis is depicted in the second row of Figure 1.

Summing Up. The entire pipeline of the proposed method could be summarized as follows:

1. Fix a subset $\mathcal{V}_{IB} = \{p_1,\dots,p_{n_{IB}}\}$ of points on $\mathcal{M}$ in order to cover the shape homogeneously.
2. Produce several Gaussian with different width around each of the the points in $\mathcal{V}_{IB}$ using the spectral Gaussian definition.
3. Obtain the basis $\mathcal{I}$ binaryizing the Gaussian functions.
4. Compute $\boldsymbol{C}$ the functional maps of dimension $k_{\mathcal{N}} \times k_{\mathcal{M}}$ between $\mathcal{M}$ and $\mathcal{N}$
5. Thanks to the spectral definition, the image of these Gaussian are easily computed on $\mathcal{N}$ using $\boldsymbol{\Phi}^{\mathcal{N}}\boldsymbol{C}$ the image of $\boldsymbol{\Phi}^{\mathcal{M}}$ via $\boldsymbol{C}$, as basis on $\mathcal{N}$.
6. Computing the sparse coefficients we can approximate and transfer functions between $\mathcal{M}$ and $\mathcal{N}$.

5. Experiments

5.1. FAUST Dataset

The FAUST dataset [BRLB14] contains 100 human shapes. All these shapes are built starting from real scans of 10 different people in a set of 10 fixed poses. The obtained collection of 100 shapes are then registered to a common template with a common triangular mesh composed by 6890 vertices and 13776 triangles. Thanks to this common template a complete ground truth point-to-point correspondence is available for all the pairs in the dataset. Among the available datasets, FAUST is one of the more recent and challenging due to the non isometric deformations generated by the different poses and subjects. We perform our experiments on these shapes using different set of 10 pairs randomly selected.

5.2. Competitors and alternatives

Standard (std). This is the classical approach based on the Fourier theory [Lév06], [VL08]. The used basis is the truncated orthonormal subset of the first eigenfunctions of the Laplace-Beltrami operator.

Standard double size (std2). The same as the the previous one but using a number of eigenfunctions equal to two times the number used in **std**.

Point-to-point mapping (p2p). We use the standard point to point map conversion with ICP proposed in the original functional map paper [OBCS*12b]. Once we have the point-to-point map we define a function on $\mathcal{N}$ assigning to each vertex of $\mathcal{N}$ the value of the original function at the corresponding vertex on $\mathcal{M}$.

Products (prod). As proposed in [NMR*18] we use not only linear combination of the eigenfunctions, instead we consider also products between pairs of them. the results is a second order polynomial representation of the functional spaces.

Geodesic Indicators (geod). This is the first of the two alternatives that we generate. In this case for each of the points in $\mathcal{V}_{IB}$ we adopt the set of indicator functions obtained from 5 different geodesic neighbourhood with 5 different levels of locality as basis. Then we perform the transfer of these geodesic indicators on the target shape using the functional map on the Fourier representation of these geodesic indicators. The analysis and synthesis of a given function is done using the two alternatives that we proposed for the IB.

Heat Indicators (heat). The last alternative is instead based on the heat kernel on the surface. In this case as indicator we use the saturated version of the heat kernel around each of the points in $\mathcal{V}_{IB}$

	approx								
dim	**std**	**std2**	**prod**	**geod (8)**	**geod**	**heat (8)**	**heat**	**ours (8)**	**ours**
10	0.70 ± 0.20	0.55 ± 0.18	0.52 ± 0.20	0.19 ± 0.06	0.18 ± 0.06	0.72	0.72	0.34 ± 0.17	0.37 ± 0.19
30	0.45 ± 0.16	0.35 ± 0.11	0.32 ± 0.10	0.19 ± 0.06	0.18 ± 0.06	0.44	0.43	0.21 ± 0.08	0.21 ± 0.09
50	0.37 ± 0.12	0.31 ± 0.09	0.27 ± 0.09	0.19 ± 0.06	0.18 ± 0.06	0.39	0.39	0.19 ± 0.07	0.19 ± 0.08
70	0.34 ± 0.10	0.28 ± 0.09	0.29 ± 0.08	0.18 ± 0.05	0.18 ± 0.6	0.36	0.38	0.18 ± 0.06	0.19 ± 0.07
90	0.32 ± 0.10	0.26 ± 0.08	0.35 ± 0.08	0.19 ± 0.07	0.18 ± 0.06	0.36	0.38	0.18 ± 0.07	0.18 ± 0.06

Table 1: *Comparison between the proposed method and the competitors in the approximation of indicator functions. The relative error computed as in Equation 14 reported in the Table is an average on 100 randomly generated indicator functions on 10 randomly selected pairs from the FAUST dataset. For each of these results we also report $\pm$ the standard deviation, except for the **heat(8)** and **heat** for which the standard deviation is always close to 0.20 or greater. Each row in the Table corresponds to a different dimension of the basis used. For each row we highlight the best result in green, the second one in red and the third one in blue.*

gt	transfer									
dim	**std**	**std2**	**p2p**	**prod**	**geod (8)**	**geod**	**heat (8)**	**heat**	**ours (8)**	**ours**
10 $\times$ 10	0.70	0.56	0.59	0.57	4.04	1.03	1.00	1.09	0.53	0.63
30 $\times$ 30	0.46	0.36	0.27	0.36	1.62	0.61	0.92	0.91	0.43	0.36
50 $\times$ 50	0.38	0.32	0.19	0.31	0.95	0.50	0.90	0.95	0.31	0.28
70 $\times$ 70	0.34	0.29	0.15	0.32	0.77	0.50	0.85	0.94	0.26	0.25
90 $\times$ 90	0.32	0.26	0.13	0.37	0.73	0.51	0.86	1.02	0.25	0.23

Table 2: *Comparison in the transfer of indicator functions between the proposed method and the competitors. The relative error computed as in Equation 15 reported in the Table is an average on 100 randomly generated indicator functions on 10 randomly selected pairs of shapes from the FAUST dataset. The functional map used for the transfer is a ground-truth functional map. Each row in the Table corresponds to a different dimension of the map **C**. For each row we highlight the best result in green, the second one in red and the third one in blue.*

for 5 different time-scales. Then the obtained basis is used as done for the geodesic indicators.

As explained in the previous Section we have two different definition for the coefficients in the proposed IB. This is true also for the **geod** and **heat** method above proposed too. In the following we will refer to the results obtained from coefficients computed as in equation 8 as **geod (8)**, **heat (8)** and **ours (8)**. While we will refer to ones obtained with Equation 9 as **geod**, **heat** and **ours**.

5.3. Evaluation details

We adopt a relative error in the approximation and transfer (respectively denoted by $\mathcal{E}_{app}$ and $\mathcal{E}_{tran}$) to give a quantitative evaluation of the results. These *relative errors* are defined as :

$$\mathcal{E}_{app} = \frac{\int_{\mathcal{M}} (f(x) - \tilde{f})^2 dx}{\int_{\mathcal{M}} f(x)^2 dx}, \tag{14}$$

$$\mathcal{E}_{tran} = \frac{\int_{\mathcal{N}} (f_{tran}(x) - \tilde{f}_{tran})^2 dy}{\int_{\mathcal{N}} f_{tran}(y)^2 dy}, \tag{15}$$

where f_{tran} is the ground truth transfer of f from $\mathcal{M}$ to $\mathcal{N}$, while $\tilde{f}$ and $\tilde{f}_{tran}$ are respectively the approximation and the transfer of the function f. In these equations dx and dy are the infinitesimal area elements respectively on $\mathcal{M}$ and $\mathcal{N}$.

5.4. Results

In all our experiment we consider a given functional map of the dimension of the basis used that are the ones selected for the method **std**. For all the methods the functional map used is the same, with its natural extension to products for the method **prod** as explained in [NMR*18]. Method **std2** is the only exception, where the dimension of the basis doubles the original one. Hence also the map has dimensions equal to two times the original dimensions.

In the first experiment, for 5 different dimensionality of the map, we compare the approximation and the transfer error for all of the competitors. The results shown are the average of 100 random indicator function on 10 random pairs from FAUST dataset. In Table 1 are reported the errors in the approximation. For each of these errors we report also the standard deviation, except for the **heat(8)** and **heat** for which the standard deviation is always close to 0.20 or greater. Being only suitable for transferring, the method **p2p** is not present in this Table. As it can be seen, the method **geod** does not depend on the dimension of the basis in the approximation and it outperforms all of the competitors when a small number of basis functions are used. On the other side the **heat** method is highly dependent on the number of eigenbasis used as it corresponds to the quality of the spectral representation of the heat diffusion. The same is true also for our method, even if it is better than the competitors except for the **geod**. Once we adopt 50 or more eigenbasis our method achieves the best approximation results also considering the standard deviation. In Table 2 we collect the results for the transfer obtained with ground truth functional maps. On each row we use a square functional map with a different dimensionality. It is clear that the geodesic information are not well transferred through the functional maps based on the LBO eigenbasis, and the precision in the geodesic approximation is completely lost. Furthermore it is clear that **ours** is more appropriate and precise with respect to **ours (8)**. Although the **p2p** achieves the best result, our performance is always fully satisfactory. Our method achieves the best results in comparison with all the other functional representation methods.

In Figure 7 we compare all the competitors on the transfer using

a ground truth functional map defined on a basis of dimension 30 on the Source shape and increasing the dimension $k_{\mathcal{N}}$ of the basis on the Target shape. On the y-axis we report the relative error computed as average of 100 random generated function on 10 random selected pairs of shapes from the FAUST dataset. On the x-axis the increasing value of $k_{\mathcal{N}}$ is shown and the last value on the right corresponds to the error in the approximation. The **p2p** achieves the best results for every value of $k_{\mathcal{N}}$. The other methods are all far from the **p2p** result, the only exception is the proposed method. As can be seen increasing the dimensionality of the basis on the target shape the results of our method are really improved. With $k_{\mathcal{N}}$ close or greater than 200 the transfer obtained with our method is not so far from the **p2p**. This confirm that the IB well represent and transfer the step functions defined on surfaces. The only limit on our basis is the quality of the map. If we have the possibility to use a larger number of eigenbasis on the target shape our method reaches the results that we have in the approximation (that are shown on the last column of the Figure 7). These results proof that our basis is the best one in the transfer application with respect to the other functional representation methods. The powerful transfer results obtained by the **p2p** is limited to the fact that this method does not constitute a functional representation, it is only useful for transfer. If we want to represent step functions on shapes with a fixed basis in a signal processing scenario we should use the proposed IB.

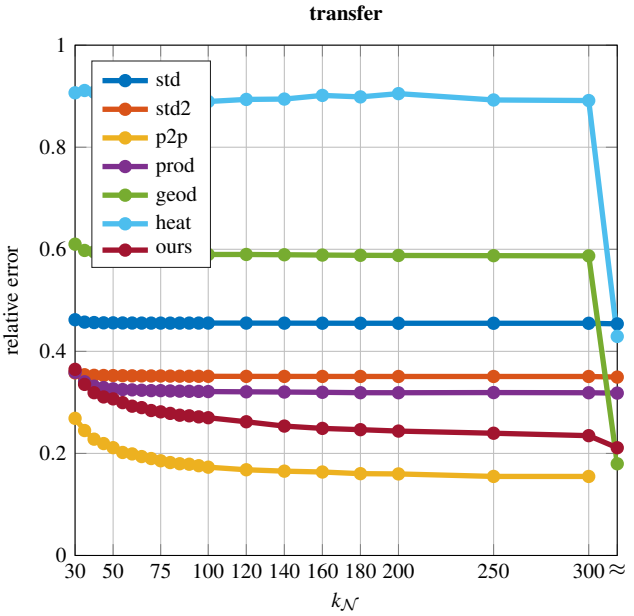

Figure 7: *Comparison on the transfer without saturation using a ground truth functional map defined on a basis of dimension* 30 *on the Source shape and varying the dimension $k_{\mathcal{N}}$ of the basis on the Target shape. The relative error computed as in Equation 15 reported in the Table is an average of 100 random generated function on 10 random selected pairs from the FAUST dataset. The last value on the x-axis correspond to the error in the approximation.*

Finally in Figure 8 some qualitative examples for the approximation and transfer of indicator functions between all the competitors are depicted. Varying the pair of shapes and the indicator function we propose three different examples. In all these experiments the functional map is encoded in a matrix of dimension 100×30. As can be seen the IB well approximates and transfers the indicator function in all the pairs considered. These qualitative results confirm again that the IB is the best functional representation for step function defined on surfaces.

	dim				
method	10×10	30×30	50×50	70×70	90×90
geod	30.72	31.00	30.74	31.10	30.71
heat	5.59	5.82	5.72	6.01	6.30
ours	0.26	0.26	0.26	0.26	0.26

Table 3: *Comparison in the timing of the three different definitions of the indicator basis **geod**, **heat** and **ours**. In the Table the time in the computation of the basis on the two shapes of each pairs. The times are reported in seconds. These are the average on 10 pairs with around 7K vertices. In each column we compare the three methods for different size of basis.*

5.5. Timing and Efficiency

In Table 3 we evaluate and compare the timing of the three alternative computations, namely **geod**, **heat** and **ours**. As it can be seen, the proposed method is definitely faster than the competitors.

6. Conclusion

In this work we propose the *indicator basis*, a new basis for the analysis of step functions defined on different domains. For the construction of this basis we provide a synthetic spectral formulation that makes it very efficient. The usefulness and the strength of the proposed basis are evaluated and compared with the state-of-the-art competitors. The proposed basis is specifically desirable for the transfer of region indicator functions. The performance in the transfer comparison confirms this claim. The quality of the obtained results and the efficiency of its computation make the indicator basis a a desirable alternative for the analysis of step functions.

Limitations. The proposed method is clearly limited by the specific set of functions for which it is defined. The indicator basis is a nice tool for the approximation and the transfer of any *step function* but can not be generalized to other functions. The proposed basis is highly dependent on the choice of parameters. For instance with a bad selection of the subset of vertices the *indicator basis* could be not able to represent indicator function on the entire surface. The analysis of the dependence between the selection of the parameters and the quality of the results may be explored as a future work.

Future work. The main point that is addressed in this paper and that follows clearly from what has been proposed is the sparse representation of *step functions* using the indicator basis. The sparse representation of functional space can be widely investigate in future work. The evaluation contained in this paper is restricted to the human shape and in particular to FAUST dataset. An extension of the present evaluation should be performed on larger set of shapes from different class and different datasets. In addition to an extensive evaluation that was not performed in this paper, also possible applications in signal processing tasks, such as localization of signals, can be explored in future work.

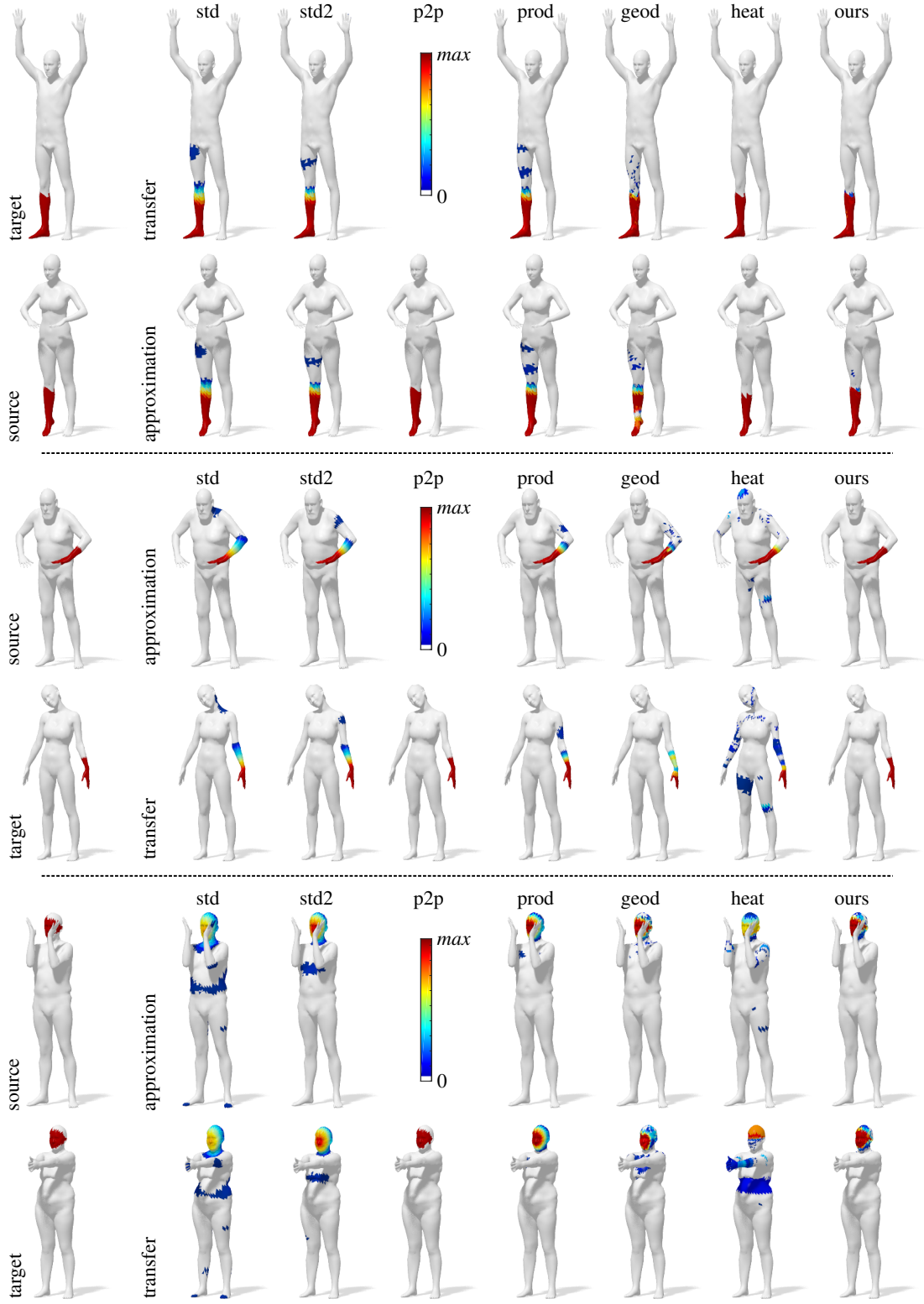

Figure 8: *A comparison between all the competitors and our indicator basis (IB) in the approximation and transfer of three different indicator functions. The Figure is divided in three sub figures. The approximation (first row) and the transfer (second row) for a different indicator function on a different pair are evaluated in each of these sub figures. The original function on the source shape and its ground truth transfer on the target shape are shown on the left. The results for all the competitors are collected on the right in the Figure. The* ***p2p*** *method does not provide results in the approximation. The colormap represents the values of the step function from* 0 *to max. The value* 0 *is represented in white in order to highlight the errors.*

Acknowledgments

We thankfully acknowledge Emanuele Rodolá, Diego Carrera, Riccardo Marin and Umberto Castellani for their valuable comments and support.

References

[ABK15] AFLALO Y., BREZIS H., KIMMEL R.: On the optimality of shape and data representation in the spectral domain. *SIAM Journal on Imaging Sciences 8*, 2 (2015), 1141–1160. 3, 4, 5

[ARAC14] ANDREUX M., RODOLÀ E., AUBRY M., CREMERS D.: Anisotropic Laplace-Beltrami operators for shape analysis. In *Proc. ECCV Workshops* (Cham, Switzerland, 2014), Springer International Publishing, pp. 299–312. 3

[ASC11] AUBRY M., SCHLICKEWEI U., CREMERS D.: The Wave Kernel Signature: A Quantum Mechanical Approach to Shape Analysis. In *Proc. ICCV Workshops* (2011), IEEE, pp. 1626–1633. 2

[BMM*15] BOSCAINI D., MASCI J., MELZI S., BRONSTEIN M. M., CASTELLANI U., VANDERGHEYNST P.: Learning class-specific descriptors for deformable shapes using localized spectral convolutional networks. *Computer Graphics Forum 34*, 5 (2015), 13–23. 3, 5

[BRLB14] BOGO F., ROMERO J., LOPER M., BLACK M. J.: FAUST: Dataset and Evaluation for 3d Mesh Registration. In *Proc. CVPR* (2014), pp. 3794–3801. 7

[CL06] COIFMAN R. R., LAFON S.: Diffusion maps. *Applied and Computational Harmonic Analysis 21*, 1 (2006), 5–30. 2

[CSBK17] CHOUKROUN Y., SHTERN A., BRONSTEIN A., KIMMEL R.: Hamiltonian operator for spectral shape analysis. *arXiv:1611.01990* (2017). 3

[dC92] DO CARMO M. P.: Riemannian geometry. *Bikhausen, Boston* (1992). 2, 4

[ELPZ97] ELDAR Y., LINDENBAUM M., PORAT M., ZEEVI Y. Y.: The farthest point strategy for progressive image sampling. *IEEE Transactions on Image Processing 6*, 9 (1997), 1305–1315. 4

[Fou07] FOURIER J.: Mémoire sur la propagation de la chaleur dans les corps solides [memoir on the propagation of heat in solid bodies]. *Nouveau Bulletin des sciences par la Société philomatique de Paris 6* (1807), 215–221. 2

[GBAL09] GEBAL K., BÆRENTZEN J. A., ANÆS H., LARSEN R.: Shape analysis using the auto diffusion function. *Computer Graphics Forum 28*, 5 (2009), 1405–1413. 2

[Kat95] KATO T.: *Perturbation Theory for Linear Operators*. Springer-Verlag, Berlin Heidelberg, 1995. 5

[KBB*13] KOVNATSKY A., BRONSTEIN M. M., BRONSTEIN A. M., GLASHOFF K., KIMMEL R.: Coupled quasi-harmonic bases. *Computer Graphics Forum 32*, 2pt4 (2013), 439–448. 3

[KGB16] KOVNATSKY A., GLASHOFF K., BRONSTEIN M. M.: MADMM: a generic algorithm for non-smooth optimization on manifolds. In *Proc. ECCV* (Cham, Switzerland, 2016), Springer International Publishing, pp. 680–696. 3

[Lév06] LÉVY B.: Laplace-Beltrami eigenfunctions towards an algorithm that understands geometry. In *Proc. SMI* (Washington, DC, 2006), IEEE, pp. 13–25. 2, 7

[MD03] MOENNING C., DODGSON N. A.: *Fast marching farthest point sampling*. Tech. rep., University of Cambridge, Computer Laboratory, 2003. 4

[MRCB16] MELZI S., RODOLÀ E., CASTELLANI U., BRONSTEIN M. M.: Shape analysis with anisotropic windowed Fourier transform. In *Proc. 3DV* (Stanford, CA, 2016), IEEE, pp. 470–478. 3, 5

[MRCB18] MELZI S., RODOLÀ E., CASTELLANI U., BRONSTEIN M. M.: Localized manifold harmonics for spectral shape analysis. *Computer Graphics Forum 37*, 6 (2018), 20–34. 3

[NMR*18] NOGNENG D., MELZI S., RODOLÀ E., CASTELLANI U., BRONSTEIN M. M., OVSJANIKOV M.: Improved functional mappings via product preservation. *Computer Graphics Forum 37*, 2 (2018), 179–190. 3, 7, 8

[NO17] NOGNENG D., OVSJANIKOV M.: Informative descriptor preservation via commutativity for shape matching. *Computer Graphics Forum 36*, 2 (2017), 259–267. 3

[NVT*14] NEUMANN T., VARANASI K., THEOBALT C., MAGNOR M., WACKER M.: Compressed manifold modes for mesh processing. *Computer Graphics Forum 33*, 5 (2014), 35–44. 3

[OBCS*12a] OVSJANIKOV M., BEN-CHEN M., SOLOMON J., BUTSCHER A., GUIBAS L.: Functional maps: a flexible representation of maps between shapes. *ACM Trans. Graphics 31*, 4 (2012), 30:1–30:11. 2, 6

[OBCS*12b] OVSJANIKOV M., BEN-CHEN M., SOLOMON J., BUTSCHER A., GUIBAS L.: Functional Maps: A Flexible Representation of Maps Between Shapes. *ACM Transactions on Graphics (TOG) 31*, 4 (2012), 30. 4, 7

[OLCO13] OZOLIŅŠ V., LAI R., CAFLISCH R., OSHER S.: Compressed modes for variational problems in mathematics and physics. *Proceedings of the National Academy of Sciences 110*, 46 (2013), 18368–18373. 3

[PP93] PINKALL U., POLTHIER K.: Computing Discrete Minimal Surfaces and their Conjugates. *Experimental mathematics 2*, 1 (1993), 15–36. 4

[Rus07] RUSTAMOV R. M.: Laplace-Beltrami eigenfunctions for deformation invariant shape representation. In *Proc. SGP* (Aire-la-Ville, Switzerland, 2007), Eurographics Association, pp. 225–233. 2

[RWP06] REUTER M., WOLTER F.-E., PEINECKE N.: Laplace–Beltrami spectra as 'Shape-DNA'of surfaces and solids. *Computer-Aided Design 38*, 4 (2006), 342–366. 2

[RZE08] RUBINSTEIN R., ZIBULEVSKY M., ELAD M.: Efficient implementation of the k-svd algorithm using batch orthogonal matching pursuit, 2008. 6

[SK14] SHTERN A., KIMMEL R.: Matching the lbo eigenspace of non-rigid shapes via high order statistics. *Axioms 3*, 3 (2014), 300–319. 3

[SOG09] SUN J., OVSJANIKOV M., GUIBAS L. J.: A concise and provably informative multi-scale signature based on heat diffusion. *Computer Graphics Forum 28*, 5 (2009), 1383–1392. 2

[SRV12] SHUMAN D. I., RICAUD B., VANDERGHEYNST P.: A windowed graph fourier transform. In *2012 IEEE Statistical Signal Processing Workshop (SSP)* (2012), pp. 133–136. 3, 5

[Tau95] TAUBIN G.: A signal processing approach to fair surface design. In *Proc. CGIT* (New York, NY, 1995), ACM, pp. 351–358. 2

[VL08] VALLET B., LÉVY B.: Spectral geometry processing with manifold harmonics. *Computer Graphics Forum 27*, 2 (2008), 251–260. 2, 3, 7